ELSEVIER

Journal of Materials Processing Technology 176 (2006) 77–86

Journal of Materials Processing Technology

www.elsevier.com/locate/jmatprotec

Simple thermo-elastic–plastic models for welding distortion simulation

P. Mollicone, D. Camilleri, T.G.F. Gray *, T. Comlekci

Department of Mechanical Engineering, University of Strathclyde, James Weir Building, 75 Montrose Street, Glasgow G1 1XJ, UK

Received 21 March 2005; received in revised form 27 February 2006; accepted 27 February 2006

Abstract

This study presents a number of finite-element (FE) models aimed at illustrating the effect of using different modelling strategies for the simulation of the thermo-elasto-plastic stages of the welding process. The main challenge with computational approaches is to model the complex and at times indeterminate nature of the welding process, preferably in a simple and transparent manner. The study uses the example of butt welding thin rectangular plates, the results of main interest being the out-of plane distortion and longitudinal residual stresses. The FE model results are compared to experimental data and simplified analytical algorithms that have been developed and validated in the context of a project to improve the prediction and control of welding distortion in thin welded structures.

Keywords: Butt welding; Distortion; Simulation; Finite-element analysis

1. Introduction

Welding is a key process in the manufacture of lightweight metallic structures in transport and in many other fields, such as box bridges, crane girders and fluid storage systems. The convenience and versatility of welding is, however, compromised by troublesome effects such as residual stresses and unwanted deformations. The latter problem leads typically to uncertainty in design and manufacture and to high rectification costs. These drawbacks are especially evident in thin plate and shell structures and have therefore inhibited progress towards lighter welded fabrication in, for example, marine craft [1] and aerospace structures [2].

Distortion and residual stress both arise from the mismatch of transient thermal strains during the passage of the heat source. The outcomes in plate structures are dominated typically by angular deformation across the line of weld, as in Fig. 1 and longitudinal contraction forces, which give rise to bending and may indeed cause buckling. Shape deviations of the work piece from the ideal, perfectly flat or regular form are strongly accentuated by the contraction forces and the distortions also accumulate in a non-linear manner as welds are added to the structure. For a given material and structural configuration, the magnitude of these effects depends primarily on the specific thermal energy input of the welding process, that is, the energy per unit length of weld. Significant reductions in distortion cannot therefore be made without changing to a welding process with less heat input and this may not always be practicable. Accurate prediction of distortion is difficult, even for simple welded structures, and is even more so for fabrications which feature several attachment welds applied consecutively.

The work described in this paper has arisen in the context of a project to improve the prediction and control of welding distortion in multiply stiffened plate structures, typical of shipbuilding practice. The increasing power and capability of computer systems mean that direct, detailed computational simulations are feasible to some extent. However, simplifications seem to be necessary in practice, as noted by Josefson [3] and Lindgren [4] and, as noted by Bachorsky et al. [5], it is important to keep computational times within a reasonable industrial time frame. Aside from the computational challenges, significant complexities arise because the thermal and mechanical properties of the weld zone and parent material are temperature-, time- and rate-dependent, and they are subject also to step variations due to material phase state changes. More particularly, these properties are not usually well characterised for a given application, nor are they straightforward to obtain experimentally.

As a first step towards simplification, the sequential, thermal-transient and thermo-elastic–plastic stages of the computation may be uncoupled without penalty, as suggested by various

* Corresponding author.
E-mail address: tom.gray@strath.ac.uk (T.G.F. Gray).

0924-0136/$ – see front matter © 2006 Elsevier B.V. All rights reserved.
doi:10.1016/j.jmatprotec.2006.02.022

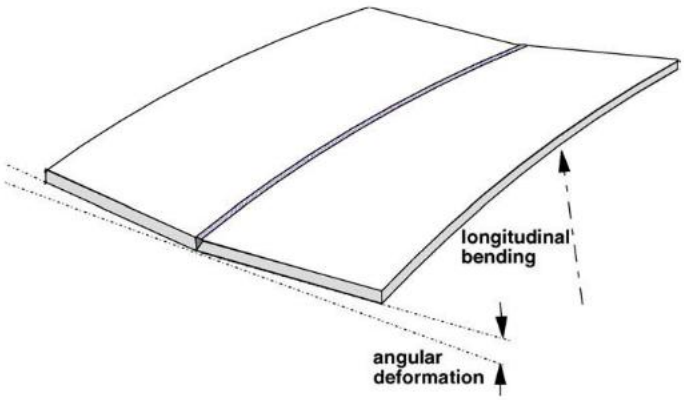

Fig. 1. Typical welding distortions.

authors [6,7]. The transient temperature field calculated in the first stage then provides input to the thermo-elastic–plastic stage. The outputs of this stage, in the form of transverse angular deformation and contraction forces, provide input in turn to an elastic finite-element analysis, which gives the final deformations in the structure.

Several researchers, including the present authors [8–10] show that the transient temperature fields can be computed adequately using finite-element methods, given some experimental support from generic welding trials. The final elastic deformations of the structure, due to the accumulation of individual welds, can also be computed relatively easily, provided that results from a thermo-elastic–plastic stage are available. The challenge, therefore, is to simplify the intractable thermo-elastic–plastic stage of the process, starting from a transient temperature field input and leading to outputs of angular deformation and a contraction stress field. The present paper explores different thermo-elastic–plastic computational models to achieve this objective and attempts to validate them against simple, analytically based formulations [10] and experimental determinations.

2. Simplified analytical model

The present authors have previously published details of simplified analytical models to predict transverse angular deformations and longitudinal contraction forces in butt welds [10,11] and in fillet welds [12,13]. These approaches were based on the early ideas of Okerblom [14]. The algorithms arising from these analyses were also incorporated into elastic finite-element models to complete the final elastic analyses of the structures. The thermo-elastic–plastic algorithms were designated 'Thermal Contraction Strain (TCS)' algorithm for angular deformation and 'Mismatched Thermal Strain (MTS)' model for longitudinal force. The details of the formulation are given in reference [10] but certain key assumptions are outlined here for completeness.

Firstly, certain characteristic features of thermal transients generated by fast-moving, intense heat sources are noted. The temperature gradient on the approach side of the thermal source is steep, as the forward heat flow rate is relatively small. For similar reasons, the temperature profile transverse to the weld is steep, whereas the gradient in the trailing region where cooling takes place is relatively shallow. Okerblom was the first to draw attention to these features and argued that the thermo-mechanical processes might therefore be modelled by considering a transverse plane strain slice, which would be passed through the quasi-stationary temperature field in the direction of welding.

In the case of the angular deformation (TCS) algorithm, the assumption is that the transverse angular deformation is dictated predominantly by contraction across the weld fusion zone, which typically varies in transverse width across thickness. The starting temperature T_s assumed for this process should correspond to level at which the material begins to develop some strength (assumed to be 1000 °C in the present case). In the sense that the TCS algorithm neglects the heating phase and assumes that an arbitrarily defined zone contracts, it is similar to the 'shrinkage volume' approach used in reference [5] and by other authors. In some cases, mechanical resistance to transverse bending and/or in-plane contraction may be provided by fixtures or clamps or by any continuous solid regions (assumed to be elastic) which are not penetrated by the fusion zone.

This is a relatively crude model but appears to provide reasonable descriptions at least in the case of single-run butt and fillet welds. The final formulation given in reference [10] expresses the transverse angular deformation θ in terms of the relative depth of penetration of the weld s/t and the relative width of the fusion zone on the surface b/t as:

$$\theta = \frac{s}{t}\frac{b}{t}\alpha T_s \left[3(1-k^2) - 2\frac{s}{t}(1-k^3)\right] \quad (1)$$

where k is a geometric parameter dependent on the shape of the fusion zone (parallel, triangular or parabolic). The specific heat input rate does not figure in this formulation, as suggested earlier, but note that the transverse *mean* contraction of the weld depends on the volume of the fusion zone and therefore on the specific heat input rate.

In the case of the longitudinal stress (MTS) algorithm, the thermal strain mismatches develop longitudinal contraction forces during the cooling phase and these spread progressively outwards as the plane strain slice passes through the transient temperature field. An important consequence of this is that the development of longitudinal stress is driven mainly by the envelope of maximum temperatures reached across the slice (see Fig. 2). Although these temperatures are reached at different times in practice, there are always mismatches at each transverse location and therefore the assumption is that it is not necessary to take account of the time offset in attaining the respective maxima. Note however, that in this approach, the contraction forces are determined by the full temperature field and not, as in the shrinkage volume approach by the behaviour of a defined region.

The longitudinal stress aspect is the most difficult to analyse in principle, due to the complexities of material behaviour mentioned earlier. However, substantial simplifications are admissible due to the fact that the longitudinal stress levels in central regions of the weld where the complex behaviour takes place are limited by the final yield strength. The authors also show [10] that the typical profile of maximum transverse temperatures is

Table 1
Comparison of experimental data, simplified MTS/TCS algorithms applied to a 3D FE model, 2D and 3D thermo-elasto-plastic models

Model ID	Average angular deformation (degrees)	Longitudinal moment (Nm)	Average curvature (m^{-1})	Computational time
Experimental data	1.73	N/A	−0.0864	N/A
TCS and MTS algorithms applied to a 3D FE Model	1.82	−63.11	−0.0604	10 min
2D Model A	0.732	−58.2	N/A	6 min
2D Model D	1.34	−108	N/A	24 min
3D Model E	4.79	−78.0	−0.108	37.5 h
3D Model G	2.39	−137	−0.151	37.5 h

inversely proportional to the distance from the centre line of the weld, approximately, and this leads to a weak dependence on the actual yield strength value, leaving the expansivity (α) as the major driving force. The expansivity and yield characteristics in an elastic-perfectly plastic model for steel are such that a relatively small temperature difference (120 °C) causes yielding in a typical case. Hence, the mechanics of contraction force development are driven primarily by the cooling phase of the cycle within a relatively low temperature range (e.g. less than 300 °C for steel) within which the material properties are likely to be fairly constant. (Expansivity values corresponding to a higher temperature range are needed for application of the TCS algorithm, due to the intervention of phase changes during cooling.)

The resulting MTS algorithm is implemented within a three-dimensional, elastic, finite-element formulation by applying a 'load' profile corresponding to an artificial temperature reduction at points across the width of the plane strain slice. In the central region, defined by thermal strain levels which exceed twice yield strain, yield magnitude tensile strain levels are applied. No loads are applied in the other regions which remain elastic, defined by thermal strain levels less than yield strain (ε_Y). In the zones between the fully plastic and elastic regions, loads corresponding to ($\alpha T_M - \varepsilon_Y$) are applied, where T_M is the maximum temperature reached at the location.

These algorithms were applied, in the studies reported earlier [9], to a 3D elastic model of a 6 mm thickness, half-metre square test geometry (two 0.25 m wide × 0.5 m long plates butt welded along the 0.5 m edges). Comparison between these results and the average experimental deformation in a batch of seven test welds is shown in the first two rows of Table 1 (the relevance of the longitudinal moment will be discussed later). The deformation comparisons are good although it should be noted that the complete results are sensitive to the temperature-dependant properties assumed.

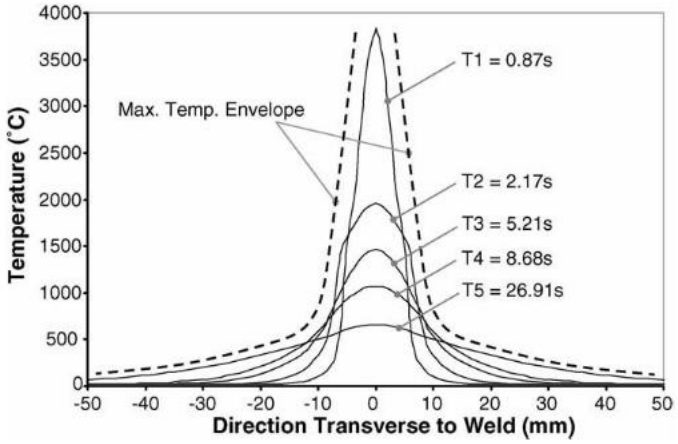

Fig. 2. Envelope of maximum temperature plots reached across a transverse slice of the plate at different times following welding.

3. Material properties

Dilatometry tests were performed by an industrial partner to obtain thermal coefficients of expansion for steel samples taken from the welds and plates under investigation.

The tests were performed at heating/cooling rates representative of the actual weld trials. Fig. 3a shows a typical plot obtained

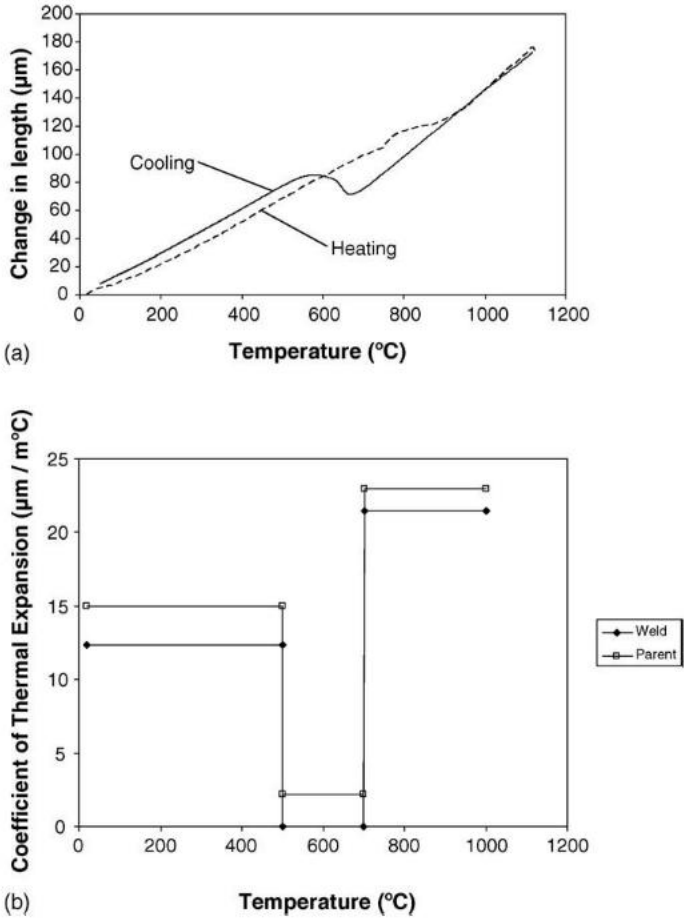

Fig. 3. (a) Typical extension vs. temperature plot obtained from dilatometer tests. (b) Coefficient of thermal expansion values extracted from dilatometer tests.

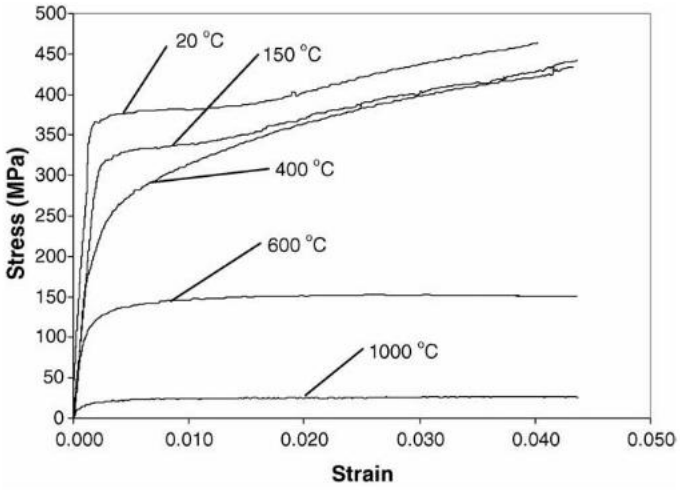

Fig. 4. Tensile testing plots for different temperatures used to extract non-linear, temperature-dependent material properties for the FE analyses.

from the dilatometer readings. The cooling part of the plot was divided into three sections to extract average temperature-dependent expansivities for both the parent and weld material (Fig. 3b). Temperature ranges within which the slope could be approximated to constant values were considered, namely: the high temperature part (down to 700 °C), the range where phase changes are evident (700–500 °C) and the final cooling to room temperature. For the FE models to which the TCS and MTS algorithms were applied, average expansivity values of 14.55 and 13.43 μm/(m °C) for the parent and weld material respectively were used.

Quasi-static tensile tests were also carried out on the test plate material at steady temperatures, ranging from ambient to 1000 °C (see Fig. 4). The results of these tests were used to determine a temperature-dependent, bilinear, strain hardening constitutive material model for the finite-element analyses. The material loses strength sharply at temperatures above 1000 °C and this value was therefore used as a cut-off temperature for the structural analyses, i.e. the maximum temperature load allowed in the structural models and the reference temperature for the computation of thermal strains of structural elements associated with the weld pool. The effective yield strength was obtained from the intersection of the elastic and plastic linear portions. Fig. 5 shows the dependence of yield strength and Young's modulus E on temperature, as extracted from the tensile testing plots.

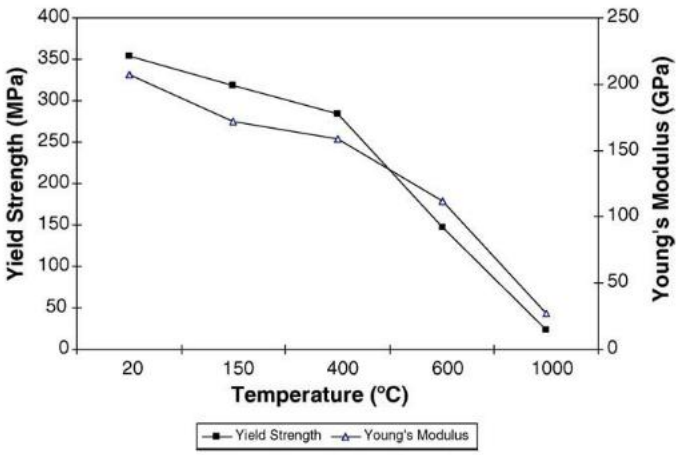

Fig. 5. Yield strength and Young's modulus used for the FE analyses.

4. Finite-element analyses

4.1. Thermal analysis

The present paper is concerned primarily with the thermo-elastic–plastic stage of the welding simulation but some discussion of the transient thermal analysis is necessary as it provides the baseline input for comparison and validation of different approaches. For gas metal arc welding processes, the complex heat transfer phenomena in the arc heating and metal transfer zone can be conveniently represented in terms of a single numerical heat source model in order to obtain the temperature history from a transient heat transfer analysis [15]. Studies in the current project have focused on CMn steel plate in the 5–8 mm thickness range and it has been shown previously [8,10] that several modelling strategies for the heat source provide equally adequate descriptions of the transient temperature fields, at least for the purposes of distortion simulation. The models previously discussed included 2D and 3D quasi-static and transient analyses, together with various thermal input models, including volumetric heat generation, Gaussian distribution of surface heat input and birth and death elements (sometimes referred to as element activation/deactivation) to simulate the incremental deposition of weld metal. These different approaches yielded similar results, at least in those regions of the model not too close to the weld centreline. Hence, a two-dimensional analysis would appear to be adequate, indicating that heat flow along the length of the weld may be neglected. This view is confirmed by the work of Nasstrom et al. [7].

In the present study, the 2D thermal analysis was carried out using a Gaussian distribution of surface heat input with an assumed weld radius of 5 mm. The 3D thermal analysis was carried out using a volumetric heat input, where the cross-sectional area was determined from a macro-section of the actual weld fusion zone (neglecting the overfill area). Although the Gaussian distribution model appears more refined, the volumetric heat input model is more suited to the meshing strategy used in the 3D analyses.

An overall temperature-dependent heat transfer coefficient was applied to the plate surfaces to include both convection and radiation, although the thermal analyses showed that most of the heat is transferred away from the weld by conduction through the plate. Other properties such as conductivity and enthalpy were taken to be temperature-dependent.

In fact, any fine differences between the alternative thermal models are greatly outweighed by uncertainty as regards the efficiency of energy conversion from the electrical input of the welding power source to thermal input energy in the particular weld configuration. In the present studies, the efficiencies were determined inversely by relating the computed thermal transients to the results obtained from an array of thermocouples. Thus, the thermal inputs to the transient profiles were based on alternative 2D or 3D thermal analyses, as described, the results of which

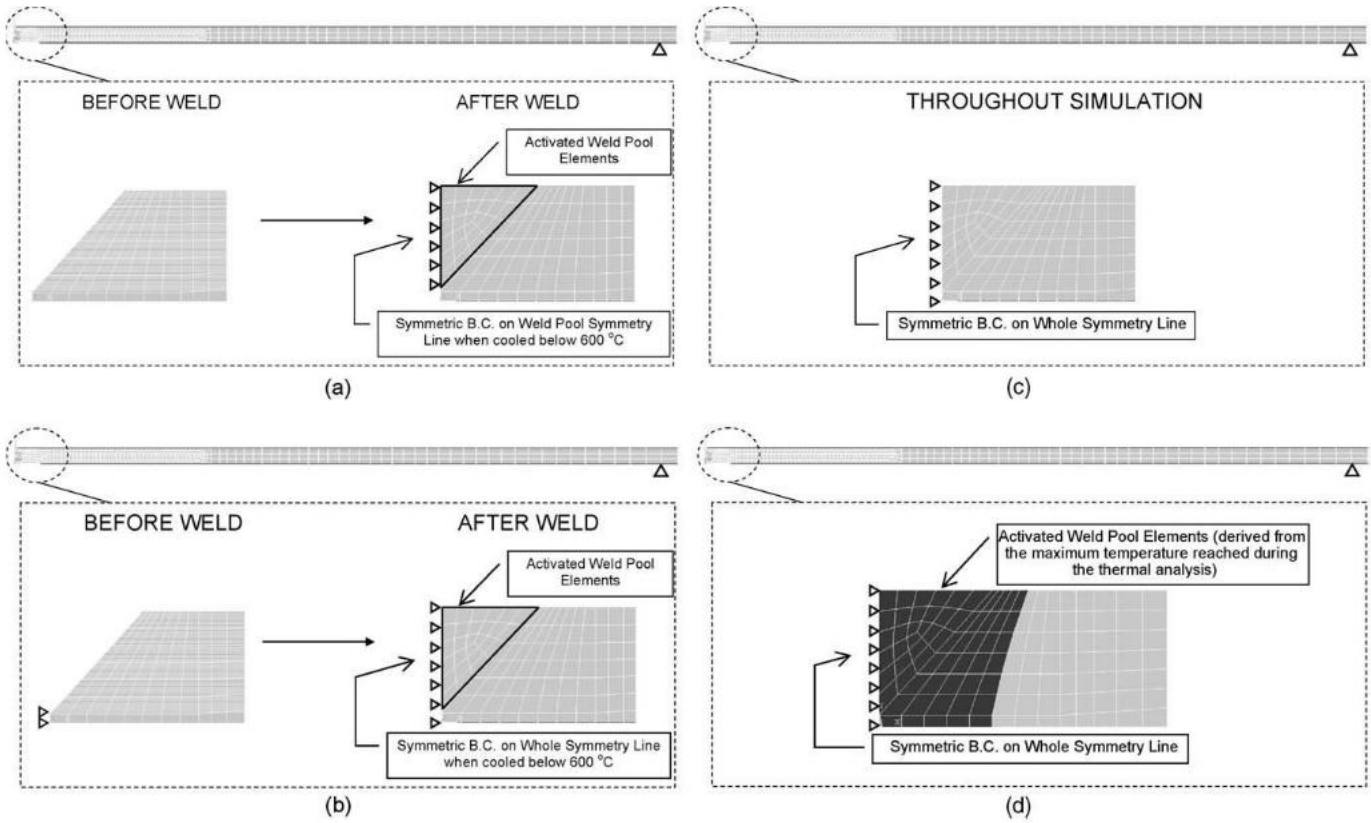

Fig. 6. (a) FE modeling strategy for 2D analysis, Model A. (b) FE modeling strategy for 2D analysis, Model B. (c) FE modeling strategy for 2D analysis, Model C. (d) FE modeling strategy for 2D analysis, Model D.

were matched to the experimental results for the corresponding test geometry. This indicated an electrical/thermal efficiency of 81% for both models. (This seems high, judging by information in the literature for a MIG process, but it may be that the flux core contributes to the input energy.) The two different models described above yielded similar transient profiles, differing only at very high temperature values for nodes within and very close to the weld fusion zone.

4.2. *Two-dimensional thermo-elasto-plastic FEA*

The plates in the computational model were supported notionally as shown at the top of Fig. 6, but additional support was provided in the experimental configuration by run-on/off tabs, which were tacked to the plates at the ends. Modelling of the symmetry conditions proved to be problematic. The fusion zone has no strength at the maximum input temperatures and the gravity loading aspect of the model had to be removed, to avoid a requirement to model the somewhat indeterminate restraint conditions imposed by the tack welded end tabs. Four different modelling approaches were tested with respect to the central boundary condition:

(A) As shown in Fig. 6(a), fusion zone elements (determined from the weld preparation shape) were activated from the onset of the input of heat energy, but the central symmetric boundary condition on these elements was activated only after cooling below 600 °C. Note that symmetry was not imposed in this model on the small 'root-face' area (see the boundary condition indicated below the element model in the figure). Hence, it was assumed that the plates were *not* continuously connected in this region, thus modelling the practical weld tests used for comparison. The angular deformation resulting from the delayed imposition of symmetry in the model was much less than typical observations (see third row of Table 1). However, the behaviour related well to the experiments in a qualitative sense, in that it was observed that the root areas on either side of the joints moved together during the welding process.

(B) Fig. 6(b) shows a variation on this condition, where the root area was assumed to be connected throughout the analysis, but other symmetry conditions were treated as in Model A. This modelling procedure yielded a slightly smaller positive angular displacement (not tabulated).

(C) Fig. 6(c) shows a model where the symmetric boundary condition was maintained throughout the thermal loading. Greater expansion of the upper part of the weld fusion zone during heating generated a negative angular displacement and a large measure of this displacement was retained on subsequent cooling to ambient temperature leading to a final negative distortion. By contrast, overall net negative angular distortion was not observed in the welding tests. When the simulated transient deformations were examined at an intermediate stage of the computational cycle, it was clear that the symmetric boundary condition was forcing the centre of the weld to slide vertically during heating. The centre-

line of the plate, as a result, lifted up during the heating part of the cycle, by an amount much greater than noted during the experiments. Although contraction of the fusion zone eventually took place during cooling, the initial overshoot was too large to result in the correct net angular distortion at the end of the transient simulation. (Incidentally, modelling the entire plate as a whole, i.e. without invoking symmetric boundary conditions, yielded the same results as the present Model C idealisation, as expected.)

(D) Fig. 6(d) shows yet a different approach where deactivation and subsequent re-activation of elements was based on the maximum temperature reached during the thermal simulation rather than on the configuration of the fusion zone obtained from experimental macro-sections. More specifically, all elements that were predicted to reach a value equal to or higher than a predefined cut-off temperature during the thermal simulation were deactivated at the start of the thermo-elasto-plastic simulation and re-activated only when they reached the cut-off temperature. For this approach the cut-off temperature was elevated to 1500 °C (approximately the liquid to solid phase transition temperature for steel) as this appeared to give better matching to the experimental behaviour. The cross-section of elements reaching the cut-off temperature does not properly match the fusion zone observed from the macro-sections but this aspect could be improved through more sophisticated treatment of the energy input distribution (to include the overfill region, among other features). Symmetric boundary conditions were maintained *throughout* this simulation with none of the adverse effects observed in Model C. The resulting angular out-of plane distortion, shown in the fourth row of Table 1, is a reasonable match to experimental data, given the various experimental uncertainties mentioned earlier.

4.3. Three-dimensional thermo-elasto-plastic FEA

The important improvement in the use of three-dimensional models is that they provide longitudinal curvature results, which are of considerable practical interest. In the TCS/MTS algorithm case shown in Table 1, the 3D model is, of course, purely elastic and has no transient thermal input or temperature-dependent thermo-elastic–plastic features. The resulting angular deformation was predicted reasonably through the TCS algorithm and the curvature was 30% less than typical experimental results as indicated.

The remaining three 3D cases considered were based on full implementation of temperature-dependent, elastic–plastic modelling and it will be noted that this implies a substantial penalty in terms of computational time. The computed time shown in Table 1 includes thermal and structural analyses and any post/pre-processing required in transferring loads from one stage to the other of the uncoupled procedure. All simulations were carried out on a dual processor Intel Xeon 2.2 GHz Workstation with 1 GB of RAM. The two-dimensional models consisted of 524 4-node ANSYS solid elements whilst the three-dimensional models consisted of 12400 8-noded ANSYS solid elements. The ANSYS sparse solver was used with a full Newton Raphson iterative solution method.

Delayed imposition of a symmetric boundary condition cannot be implemented in these models, as it is incompatible with incremental travel of the heat source providing the transient thermal input. As with the 2D analyses, birth and death elements were used to improve simulation of weld material deposition. Due to the highly non-linear nature of the simulations (non-linear material properties and geometry) and the wide range of temperature loading, non-convergence problems were encountered. These were dealt with by adjusting:

- mesh density to reach a suitable compromise between element size and computational time;
- time intervals for load-steps;
- the criterion for re-activation of the weld pool elements as the transient temperature field advanced along the plate. The aim was to make sure that elements were not re-activated until the entire element volume reached temperatures equal to or higher than the cut-off temperature.

In the first two 3D models (E and F), shown in Fig. 7, the elements representing the fusion zone were assigned a reference temperature equal to the cut-off temperature (taken to be 1000 °C for Models E and F) in order to simulate the contraction thermal strain during the cooling cycle. The difference between the models then lies in the boundary conditions, as follows:

(E) The symmetric boundary condition was applied in the root-face area only as shown in Fig. 7(a). The correct pattern of deformation was obtained from this model, but the computed angular deformation and longitudinal curvature were much greater than the experimental benchmarks (see Table 1).

(F) Fig. 7(b) shows the case where the symmetric boundary condition was applied across the whole thickness (3D version of 2D Model C). The resulting angular deformations took place in a similar sense to Model C, i.e. showing negative final curvature. This result did not match the experimental results and therefore is not shown in Table 1.

(G) Model G is the three-dimensional analogue of the two-dimensional Model D, as the same strategy was used for the activation and deactivation of elements: all elements observed to reach a value equal to or higher than a predefined cut-off temperature during the thermal simulation were deactivated at the start of the thermo-elasto-plastic simulation and re-activated only when they reached the cut-off temperature. Similarly to Model D, the cut-off temperature was elevated to 1500 °C and symmetry boundary conditions were maintained throughout this simulation across the whole thickness. Compared to the other three-dimensional Models E and F, this approach gave better results for angular distortion. The resulting longitudinal curvature was similar to the other elasto-plastic models but rather greater than the experimental data. These results are shown in the final row of Table 1.

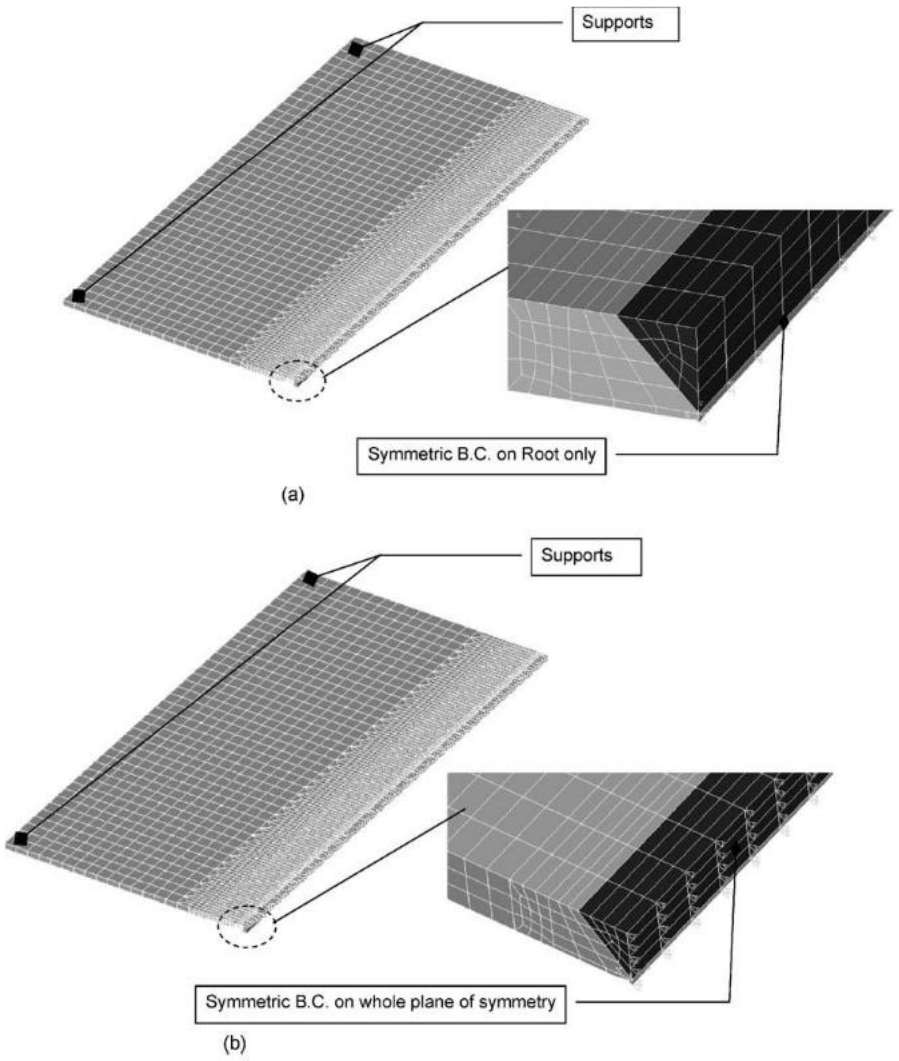

Fig. 7. (a) FE modeling strategy for 3D analysis, Model E. (b) FE modeling strategy for 3D analysis, Model F.

4.4. Longitudinal stress development

The differences in outcomes between the different formulations, particularly for the longitudinal bending deformation (average curvature) arise from differences in the simulated angular distortion on the one hand and the development of longitudinal stress on the other. It is therefore of interest to compare the final longitudinal residual stress distributions arising from different models, i.e. the best of the 2D thermal and structural models, the best of the 3D models and the analytical approach. The longitudinal contraction force is also relevant to the risk of buckling deformation. A comparison of stress distributions is shown in Fig. 8 (in the case of the 3D simulations, the comparison is based on the longitudinal stress at mid-thickness and at mid-length). The residual stresses give rise to longitudinal bending moments, shown in Table 1. These depend also on the cross-sectional shape. A large angular deformation results in a large bending moment for a given net contraction force but, as the bending stiffness of the plate is then higher, this compensates and results in less variation in the predicted final curvatures.

The 2D Model D gives a very close result to the MTS algorithm for longitudinal contraction stress pattern (Model A is very similar) apart from the obvious difference that the computational model includes the temperature-dependent work-hardening property which causes residual stresses in excess of the room temperature yield strength (also noted in experimental work such as [16].) This tends to confirm key simplifying

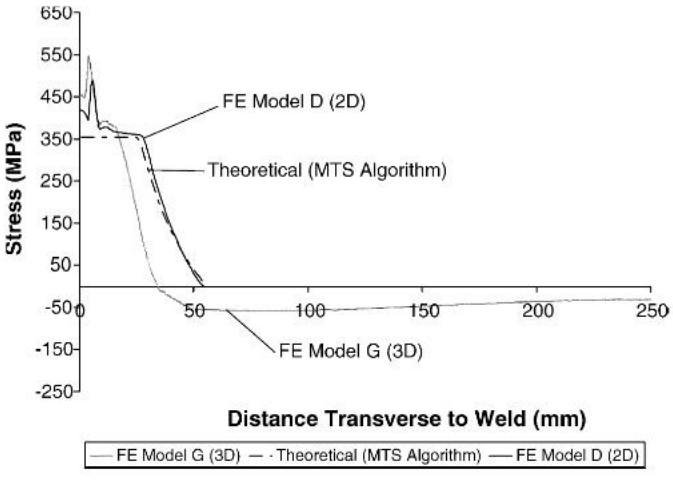

Fig. 8. Comparison of longitudinal residual stresses.

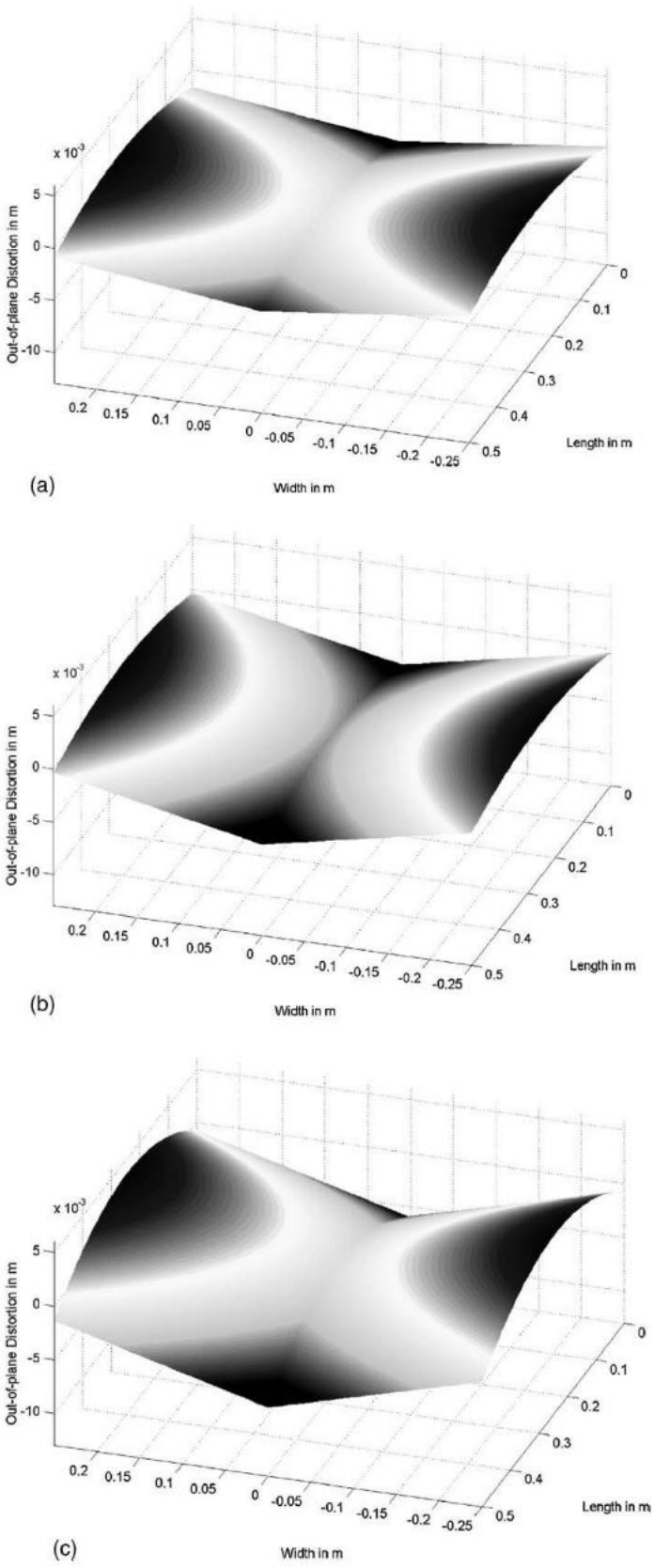

Fig. 9. (a) Experimental results [8]: out-of plane distortion. (b) TCS and MTS algorithm applied to 3D FE Model: out-of plane distortion. (c) 3D FE elasto-plastic Model G: out-of plane distortion.

assumptions embodied in the MTS algorithm, namely, that the maximum temperature at each transverse location is indeed the important driving parameter and that the longitudinal offset of these maxima due to the time interval may be ignored, as indicated earlier in Section 2. In both of these cases, the plane strain residual stress profiles relax in the following FE analysis to satisfy equilibrium (when the 'initial strain' load profiles are applied to the 3D elastic analysis.) In the case of the full three-dimensional models, the necessary equilibrium balance of tensile and compressive longitudinal stress is obtained automatically.

4.5. Out-of plane distortion

Fig. 9 shows a comparison of the final out-of plane distortions obtained for:

(a) experimental data (the computational analyses are compared with the net out-of plane experimental profiles, i.e. the final shape of the plate minus the initial shape prior to welding, as the FE models are based on the assumption of an initially flat plate);
(b) three-dimensional FE elastic model using the simplified analytical algorithms as input;
(c) three-dimensional thermo-elasto-plastic FE Model G.

As mentioned in the model descriptions, the three-dimensional FE Model G yielded an out-of plane distortion pattern similar to the experimental and algorithm-based values, but with slightly higher centreline values at the plate ends. This might be due to the absence of the run-on/off tabs in the modelling of the welded plates.

5. Discussion

This investigation has focused on the thermo-elastic–plastic stage of welding distortion simulation, with the objectives, firstly, to find simple finite-element modelling approaches that match experimental data reasonably and secondly, to compare the results with a simple analytical strategy, which circumvents the problematic thermo-elastic–plastic stage of computation. It is assumed that the same starting point is used in each case, namely, the results of a thermal analysis or an experimental temperature field.

The key output indicators for modelling strategies in the case of out-of plane distortion are the angular deformation, which determines the cross-sectional shape and the longitudinal stress development, which determines the longitudinal curvature and buckling characteristics.

5.1. Angular contraction

The analytical strategy embodied in the TCS algorithm is based on a 2D view of the angular contraction process, together with an assumption that the prior expansion phase is either insignificant or is suppressed by structural constraint. This algorithm predicted the experimental angular distortions well in

the earlier studies [9], although it should be admitted that this accuracy depends on the choice of expansivity property for the material. It is also noted in reference [9] that the experimental angular contraction depended on the root boundary conditions, i.e. whether the plates were effectively separate but connected through weld tacks or whether the groove had been machined in a single plate to give a continuously connected root. In the latter case, higher angular deformations were observed.

It might be expected that, as Model A follows the same assumption for the fusion zone shape as the TCS algorithm, which gave reasonable correspondence with the experimental results, Model A should also give reasonable prediction. However, Model A underestimates the angular deformation. The critical difference between the TCS algorithm and the elasto-plastic analysis is that the former ignores the heating phase or at least assumes that tack welds or other restraints are sufficient to prevent negative angular deformation at this stage. This gives rise to a smaller net angular deformation in the elasto-plastic analysis.

However, Model D, which treats the high temperature zone in a different way, removes the need for imposition of a problematic boundary condition and improves prediction substantially. The surprising feature is that both 2D models are indeed so effective, in that the 2D cross-section would not seem to be free in practice to move independently of the surrounding 3D structure. The reason may be that the plate ahead of the welding arc is free to rotate (as there is as yet no weld in place) and the incremental nature of the process means that the region behind the weld is also cooling and rotating in the same sense as the fusion zone. All 2D models are, of course, economical in computational time and substitution of Model D for the TCS algorithm would not create a large penalty.

The better of the two 3D simulations (Model G) over-predicts the angular deformation, probably because it is difficult to model the central region in a simple manner.

5.2. *Longitudinal distortion*

Longitudinal distortion is driven by the longitudinal stress development and Fig. 8 shows that the MTS algorithm and 2D Model predictions agree closely. The longitudinal moment depends on the combination of longitudinal force pattern and cross-sectional shape, as does the curvature, and it is of interest that the longitudinal moments in Table 1 are fairly similar, except for Model G. All of the thermo-elasto-plastic modelling approaches shown over-predict the curvature (especially the 3D models) but this is mostly due to the over-prediction of angular deformation.

6. Conclusion

The following observations and conclusions can be drawn from the results:

(1) All results bear out the critical simplifying assumptions that the peak temperature reached at a given transverse location is the primary driver for the distortion process and the longitudinal offset in distance and time of these peaks may be ignored. (That is, a two-dimensional, time-independent thermal model seems to be adequate, at least for the typical thermal and process parameters of the example problem.)

(2) The close match between the longitudinal residual stress patterns generated by the MTS algorithm and the elasto-plastic models tends to substantiate the assumption embodied in the analytical approach whereby elastic, temperature independent, material strength properties are considered sufficient. As the analytical approach is then developed through linear elastic finite-element analyses it is a more computationally efficient method compared to the full elasto-plastic modelling approach.

(3) The temperature-dependent yield strength property incorporated in the elasto-plastic models did not have a strong influence on development of the residual longitudinal stresses. The central residual stress level depended almost entirely on the ambient temperature yield strength, with only slight increases close to the weld axis due to the inclusion of strain hardening in the FE material model. Taking the area of the stress vs. transverse distance plot as a representative of the contraction force imposed by the residual stresses (this being the driving force for longitudinal bending or buckling), the increase of force over the MTS algorithm model, due to strain hardening, is only 8%, approximately. Some allowance for this could easily be included in the MTS model.

Acknowledgements

Financial support was provided from EPSRC Grant no. GR/R335407/01. BAE Systems Marine Ltd. Govan are thanked for welding equipment, material and moral support. The dilatometer results were kindly supplied by Corus Ltd.

References

[1] T.D. Huang, P. Dong, L.A. DeCan, D.D. Harwig, Residual stresses and distortions in lightweight ship panel structures, Northrop Grumman, Technol. Rev. J. 11 (1) (2003) 1–26.
[2] B. Irving, Why aren't airplanes welded? Welding J. (January) (1997) 31–41.
[3] B.L. Josefson, et al., Welding residual distortions in ring-stiffened pipes, J. Offshore Mech. Arctic Eng. (1996) 118.
[4] L.E. Lindgren, Finite element modelling and simulation of welding. Part 1. Increased complexity, J. Therm. Stress. 24 (2001) 141–192.
[5] A. Bachorsky, M.J. Painter, A.J. Smailes, M.A. Wahab, Finite-element prediction of distortion during gas metal arc welding using the shrinkage volume approach, J. Mater. Process. Technol. 9293 (1999) 405–409.
[6] Y. Ueda, K. Nakacho, Simplifying methods for analysis of transient and residual stresses and deformations due to multipass welding, Trans. JWRI (Osaka, Japan) 11 (1) (1982) 95–103.
[7] M. Nasstrom, L. Wikander, L. Karlsson, L.E. Lindgren, J. Goldak, Combined 3-D and shell element modelling of welding, in: IUTAM Symposium on the Mechanical Effects of Welding, Luleå, Sweden, 1991, pp. 10–14, pp. 197–206.
[8] D. Camilleri, T. Comlekci, C.K. Lee, H. Tan, T.G.F. Gray, Investigation of temperature transients during flux-cored CO2/Ar Butt Welding of CMn Steel Plates, in: Proceedings of the International Conference on Metal Fabrication and Welding Technology, METFAB, September, 2003, pp. 107–116.

[9] D. Camilleri, T. Comlekci, T.G.F. Gray, Out-of plane distortion of CMn steel plates during flux-cored CO2/Ar automatic butt welding, in: Proceedings of the International Conference on Metal Fabrication and Welding Technology, METFAB, September, 2003, pp. 117–127.
[10] D. Camilleri, T. Comlekci, T.G.F. Gray, Computational prediction of out-of-plane welding distortion and experimental investigation, J. Strain Anal. 40 (2) (2005) 161–170.
[11] D. Camilleri, T.G.F. Gray, Computational efficient welding distortion simulateon techniques, Modell. Simul. Mater. Sci. Eng. 13 (2006) 1365–1382.
[12] D. Camilleri, T. Comlekci, T.G.F. Gray, Thermal distortion of stiffened plates due to fillet welds—computational and experimental investigation, J. Therm. Stress. 29 (2) (2006) 111–137.
[13] D. Camilleri, T. Comlekci, T.G.F. Gray, Design support tool for prediction of welding distortion in multiply-stiffened plate structures: experimental and computational investigation, J. Ship Prod. 21 (4) (2005) 219–234.
[14] N.O. Okerblom, The Calculations of Deformations of Welded Metal Structures, Her Majesty's Stationery Office, London, 1958.
[15] M.A. Wahab, M.J. Painter, M.H. Davies, The prediction of the temperature distribution and weld pool geometry in the gas metal arc welding process, J. Mater. Process. Technol. 77 (1998) 233–239.
[16] A. Paradowska, J.W.H. Price, R. Ibrahim, T. Finlayson, A neutron diffraction study of residual stress due to welding, J. Mater. Process. Technol. 164–165 (2005) 1099–1105.